2024 IEEE/RSJ International Conference on Intelligent Robots and Systems (IROS)
October 14-18, 2024. Abu Dhabi, UAE

Whole-body Compliance Control for Quadruped Manipulator with Actuation Saturation of Joint Torque and Ground Friction

Tianlin Zhang, Xuanbin Peng, Fenghao Lin, Xiaogang Xiong†, and Yunjiang Lou

***Abstract*— In normal operations, when quadruped manipulators with impedance control experience external disturbances, they may become unstable and lose balance due to actuation saturation, affecting their stability, safety, and compliance with the environment. To address this issue, we propose a whole-body compliance controller to prevent unstable behaviors like slip, oscillation, and overshoot, which arise from actuation saturation. The controller includes an admittance scheme with a set-valued operator as the internal feedback, to constrain joint torques within actuators' limits and ground reaction forces within friction cones to ensure stability against disturbances. Then, it formulates a hierarchical optimization problem using the Hierarchical Quadratic Programming (HQP) to impose the output of the admittance scheme while ensuring physical consistency to maintain compliance behaviors. Unlike traditional compliance control with one-dimensional torque limitations, our approach considers both joints torque limits of manipulator joints and friction cones of quadruped ground reaction as actuation saturation. This ensures overall compliance and stability for the quadruped manipulators, even under significant external forces, regardless of where they are exerted on the robot. We demonstrate through experiments involving variable stiffness environments and external forces during normal operations how effective our approach is in enhancing the safety of quadruped manipulators.**

I. INTRODUCTION

The quadruped manipulator, shown in Fig. 1, is a versatile platform consisting of a mobile quadruped and a manipulator. Its advantage lies in its ability to interact with and modify the environment, which is crucial for Human-Robot Interaction (HRI) [1]–[3]. However, due to hardware limitations and stability requirements for legged robots (i.e., friction cone [4]), sudden external forces from the environment (e.g., changes in payload or contact with stiff surfaces) can cause its actuation saturation. This includes actuators' torque limits and the stability margin edge in the friction cone. Such situations lead to undesirable behaviors like slips, oscillations, and overshoots that may damage robot hardware or surrounding objects and even injure people. Therefore, achieving compliance with quadruped manipulators for saturated cases is an important HRI task.

†Corresponding author

*This paper is supported in part by the Shenzhen Science and Technology Programs under Grants KQTD 20190929172545139 and GXWD 20231130153844002, and partially supported by GuangDong Basic and Applied Basic Research Foundation 2022A1515011521.

T. Zhang, X. Peng, F. Lin, X. Xiong, and Y. Lou are with the School of Mechanical Engineering and Automation, Harbin Institute of Technology Shenzhen, Shenzhen 518000, Guangdong, P. R. China. (email: skywoodszcn@gmail.com; xuanbin.peng@gmail.com; 15928746119@163.com; {xiongxg, louyj}@hit.edu.cn).

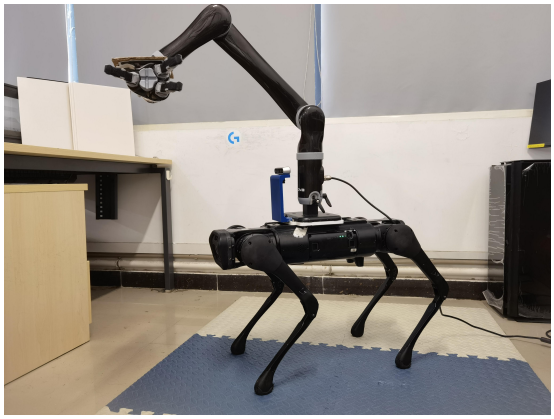

Fig. 1. An illustration of a quadruped manipulator consisted of an Aliengo platform of quadruped robot and one 6-DOF Kinova manipulator.

Legged robots have widely used compliance control, including impedance and admittance control, as reported in previous studies [5]–[8]. Compliance control allows the robot to specify the force produced in response to environmental motion by setting the impedance (i.e., stiffness and damping). However, it is a trade-off between task performance and robustness against unexpected environmental interactions. High impedance improves tracking performance and disturbance rejection but can lead to actuation saturation when the quadruped manipulator comes into contact with a highly stiff environment, such as a rigid wall. It may generate commands that are out of the robot's motion and violate stability conditions, leading to slipping [9]. Decreasing impedance prevents actuation saturation but results in poor responsiveness against contact forces, making it unsuitable for many applications [10]. An alternative approach is to model torque limits and stability requirements as constraints of linear inequalities combined with the whole-body controller (WBC) [11]–[13] in order to ensure that these constraints are not violated. However, WBC is unable to eliminate snapping-back behaviors that result from actuation saturation, with can cause overshoots and oscillations. This becomes particularly problematic when a large external disturbance force is applied to the robot's body or base, where using any force sensor is difficult or impossible. In such cases, significant deviations between the robot and commands can lead to unpredictable behaviors under actuation saturation.

These unsafe problems caused by actuation saturation have received widespread attention recently. To be specific, the work in [14]–[16] employed the proxy-based sliding mode control (PSMC) to achieve a smooth and overdamped recov-

ery from the saturation in the compliance control, thereby avoiding unsafe behaviors. Moreover, the work in [17] and [18] utilized the mathematical transformation between the set-valued signum function and a nonsmooth operator (i.e., the set-valued normal cone) to allow for more quicker desaturating. This method is equivalent to the conventional compliance control as long as the actuator torque is unsaturated but yields external force without overshoots or oscillations when the torque is saturated. However, since linear controllers (e.g., proportional-derivative-integral (PID) position controller) are widely used among these methods, they may not perform well for nonlinear systems or even violate physical consistency. Meanwhile, they are limited to one-dimensional systems and cannot be extended to multi-dimensional robots like the quadruped manipulator, which are more prone to instability due to the coupling influence of each joint and long-link chain. In particular, the motion of quadruped manipulators is coupled with locomotion and manipulation [19], requiring controllers to consider full system states.

This manuscript proposes a whole-body compliance controller for the quadruped manipulator to avoid unsafe behaviors (e.g., slips, oscillations, and overshoots) caused by actuation saturation due to external disturbances, inspired by [15] and [17]. The method considers actuator torque limits of manipulator and friction cone of ground reaction force of the legged body as actuation saturation and stability requirements. To eliminate coupling effects, locomotion and manipulation are decoupled into independent subsystems. Then, an admittance scheme with a set-valued normal cone is designed to prevent unsafe behaviors due to actuation saturation. Finally, a hierarchical optimization problem is formulated to impose the admittance scheme's output for the robot while satisfying physical consistency. As a results, the proposed methods enables the robot to be stabilized under large external force disturbances, regardless of whether the force is exerted on force/torque sensors.

This work offers the following contributions:

- This manuscript presents a new method for whole-body compliance control for multi-dimensional systems under actuation saturation, particularly the quadruped manipulator. The method ensures the robot's stability under large external force disturbances, regardless of its exerted point on the robot.
- To prevent unsafe behaviors such as slip, oscillation, and overshoots caused by the actuation saturation, the method considers both the torque limitations and friction cone of ground reaction for legged robots as forms of saturation to enhance the overall stability.
- The proposed method has been validated through various experiments and compared with previous methods. Additionally, it has been made open source[1].

To the best of the authors' knowledge, this is the first time to solve the actuation saturation problem for quadruped manipulators.

[1]The code is available at https://github.com/skywoodsz/qm_control

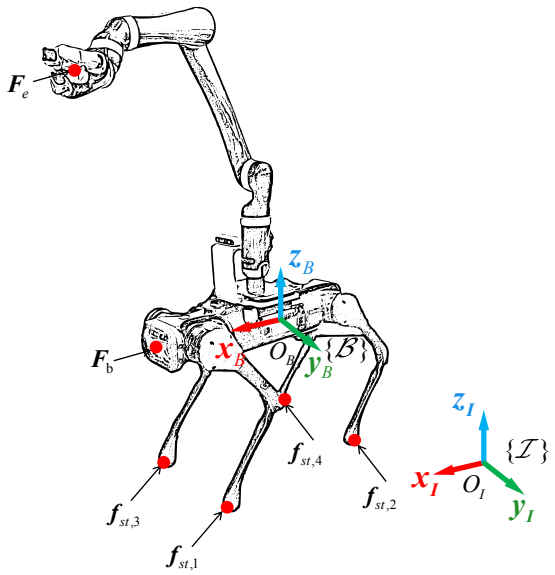

Fig. 2. The quadruped manipulator's frames (inertial $\mathcal{I}$, base $\mathcal{B}$), external contact wrench $\boldsymbol{F}_e$, $\boldsymbol{F}_b$, and ground reaction forces $\boldsymbol{f}_{st,i}$ subjected to the friction cone.

II. PROBLEM FORMULATION

A. System Modelling

In Fig. 2, the frames of a quadruped manipulator are shown. Then, the dynamics of the quadruped manipulator can be described using the two frames: the right-hand inertial coordinate frame $\{\mathcal{I} : O_I - \boldsymbol{x}_I\boldsymbol{y}_I\boldsymbol{z}_I\}$ and the body frame $\{\mathcal{B} : O_b - \boldsymbol{x}_b\boldsymbol{y}_b\boldsymbol{z}_b\}$:

$$\underbrace{\begin{bmatrix} \boldsymbol{M}_b & \boldsymbol{M}_{bl} & \boldsymbol{M}_{ba} \\ \boldsymbol{M}_{lb} & \boldsymbol{M}_l & \boldsymbol{M}_{la} \\ \boldsymbol{M}_{ab} & \boldsymbol{M}_{al} & \boldsymbol{M}_a \end{bmatrix}}_{\boldsymbol{M}} \underbrace{\begin{bmatrix} \ddot{\boldsymbol{q}}_b \\ \ddot{\boldsymbol{q}}_l \\ \ddot{\boldsymbol{q}}_a \end{bmatrix}}_{\dot{\boldsymbol{v}}} + \underbrace{\begin{bmatrix} \boldsymbol{n}_b \\ \boldsymbol{n}_l \\ \boldsymbol{n}_a \end{bmatrix}}_{\boldsymbol{n}} = \boldsymbol{J}_b^T \boldsymbol{F}_b + \underbrace{\begin{bmatrix} \boldsymbol{J}_{st,b}^T \\ \boldsymbol{J}_{st,l}^T \\ \boldsymbol{0}_{n_a \times 3n_c}^T \end{bmatrix}}_{\boldsymbol{J}_{st}^T} \boldsymbol{F}_{st} + \underbrace{\begin{bmatrix} \boldsymbol{J}_{e,b}^T \\ \boldsymbol{0}_{n_l \times 6}^T \\ \boldsymbol{J}_{e,a}^T \end{bmatrix}}_{\boldsymbol{J}_e^T} \boldsymbol{F}_e + \underbrace{\begin{bmatrix} \boldsymbol{0}_{6\times 1} \\ \boldsymbol{\tau}_l \\ \boldsymbol{\tau}_a \end{bmatrix}}_{\boldsymbol{\tau}} \tag{1}$$

where $\boldsymbol{M}$ is the inertia matrix, $\boldsymbol{n}$ represents the nonlinear effects (i.e., Coriolis, centrifugal, and gravitational terms), $\dot{\boldsymbol{v}} = [\ddot{\boldsymbol{q}}_b^T, \ddot{\boldsymbol{q}}_l^T, \ddot{\boldsymbol{q}}_a^T]^T \in \mathbb{R}^{6+n_l+n_a}$ is the stacked vector of generalized accelerations, a ZYX-Euler angle parameterization is assumed to represent the base's orientation, the subscripts b, l, a and e stand for the base, legs, arm and arm's end-effector, respectively, n_l, n_a, n_c denote the number of DoFs of leg, arm, and contact feet, respectively, $\boldsymbol{F}_b = \left[\boldsymbol{f}_b^T, \boldsymbol{\tau}_b^T\right]^T \in \mathbb{R}^6$ denotes the external wrench acting on the base, $\boldsymbol{F}_{st} = [\boldsymbol{f}_{st_1}^T, \boldsymbol{f}_{st_2}^T, \cdots, \boldsymbol{f}_{st_{n_c}}^T]^T \in \mathbb{R}^{3n_c}$ are the ground reaction forces, $\boldsymbol{F}_e = \left[\boldsymbol{f}_e^T, \boldsymbol{\tau}_e^T\right]^T \in \mathbb{R}^6$ denotes the external wrench acting on the arm's end-effector, $\boldsymbol{J}_b$, $\boldsymbol{J}_{st}$ and $\boldsymbol{J}_e$ are matrix of stacked contact Jacobians defined by base, contact feet and arm's end-effector, respectively, and $\boldsymbol{\tau}$ is the vector of actuators' torques.

Transforming the dynamics (1) into the operational space [20], one has:

$$\boldsymbol{\Lambda}(\boldsymbol{x})\ddot{\boldsymbol{x}} + \boldsymbol{\mu}(\boldsymbol{x},\dot{\boldsymbol{x}})\dot{\boldsymbol{x}} + \boldsymbol{F}_g = \boldsymbol{F}_\tau + \boldsymbol{F}_e + {\boldsymbol{J}_e}^{-T}\boldsymbol{J}_b^T\boldsymbol{F}_b \quad (2)$$

where $\boldsymbol{x} \in \mathbb{R}^6$ is the arm's end-effector pose expressed in the inertial frame, $\dot{\boldsymbol{x}} = \boldsymbol{J}_e\boldsymbol{v}$, $\ddot{\boldsymbol{x}} = \dot{\boldsymbol{J}}_e\boldsymbol{v} + \boldsymbol{J}_e\dot{\boldsymbol{v}}$, $\boldsymbol{F}_g \in \mathbb{R}^6$ is the gravity, $\boldsymbol{\Lambda}(\boldsymbol{x}) = {\boldsymbol{J}_e}^{-T}\boldsymbol{M}{\boldsymbol{J}_e}^{-1} \in \mathbb{R}^{6\times6}$ represents Cartesian inertia, $\boldsymbol{\mu}(\boldsymbol{x},\dot{\boldsymbol{x}}) = {\boldsymbol{J}_e}^{-T}\left(\boldsymbol{n} - \boldsymbol{M}{\boldsymbol{J}_e}^{-1}\dot{\boldsymbol{J}}_e\right){\boldsymbol{J}_e}^{-1} \in \mathbb{R}^{6\times6}$ represents Cartesian Coriolis and centrifugal matrix, and $\boldsymbol{F}_\tau = {\boldsymbol{J}_e}^{-T}\boldsymbol{\tau} + {\boldsymbol{J}_e}^{-T}\boldsymbol{J}_{st}^T\boldsymbol{F}_{st} \in \mathbb{R}^6$ is the input force. Therefore, the input force is composed of actuators' torques $\boldsymbol{\tau}$ and the ground reaction forces $\boldsymbol{F}_{st}$.

B. Problem Statement

To actively contact with environments with compliance, the manipulator's end-effector first needs to behave as a constrained mass-damper-spring system [21] as follows:

$$\boldsymbol{F}_e = \boldsymbol{\Lambda}_d\ddot{\tilde{\boldsymbol{x}}} + \left(\boldsymbol{\mu}(\boldsymbol{x},\dot{\boldsymbol{x}}) + \boldsymbol{D}_d\right)\dot{\tilde{\boldsymbol{x}}} + \boldsymbol{K}_d\tilde{\boldsymbol{x}} \quad (3a)$$

$$s.t.\ \boldsymbol{\tau}_{\min} \le \boldsymbol{\tau} \le \boldsymbol{\tau}_{\max} \quad (3b)$$

$$\boldsymbol{F}_{st} \in \boldsymbol{\mathcal{C}} \quad (3c)$$

where $\boldsymbol{\mathcal{C}}$ is the friction cone between the robot feet and ground, $\boldsymbol{\Lambda}_d \in \mathbb{R}^{6\times6}$, $\boldsymbol{D}_d \in \mathbb{R}^{6\times6}$ and $\boldsymbol{K}_d \in \mathbb{R}^{6\times6}$ are the desired Cartesian inertia, damping and stiffness, respectively, while $\ddot{\tilde{\boldsymbol{x}}} = \ddot{\boldsymbol{x}} - \ddot{\boldsymbol{x}}_d$, $\dot{\tilde{\boldsymbol{x}}} = \dot{\boldsymbol{x}} - \dot{\boldsymbol{x}}_d$, and $\tilde{\boldsymbol{x}} = \boldsymbol{x} - \boldsymbol{x}_d$ are errors of the acceleration, velocity and position, respectively. The actuation saturation is composed of actuators' torque limits (3b) based on the hardware and friction cone constraints (3c) to avoid slipping.

Without loss of generality, we assume that the interaction wrench $\boldsymbol{F}_e$ at the arm's end-effector is measurable, since a force sensor can be easily attached, while the interaction wrench at the base $\boldsymbol{F}_b$ is immeasurable. Moreover, the desired acceleration $\ddot{\boldsymbol{x}}_d$, velocity $\dot{\boldsymbol{x}}_d$, and position $\boldsymbol{x}_d$ are known smooth functions defined by the operators. The controller's objective is to achieve an improved postsaturation behavior, ensuring the quadruped manipulator's stability when actuators' torques $\boldsymbol{\tau}$ reach limits as in (3b) or stand forces $\boldsymbol{F}_{st}$ reaches to the friction limits as in (3c), caused by external force disturbances.

III. Proposed Controller Design

A. Admittance scheme with set-valued operator

As the interaction wrench at the base $\boldsymbol{F}_b$ is immeasurable, $\boldsymbol{F}_b$ can be regarded as an unknown disturbance. Taking (3a) into (2) and making $\boldsymbol{\Lambda}_d = \boldsymbol{\Lambda}(\boldsymbol{x})$, we have

$$\boldsymbol{F}_\tau = \boldsymbol{F}_g + \boldsymbol{\Lambda}(\boldsymbol{x})\ddot{\boldsymbol{x}}_d + \boldsymbol{\mu}(\boldsymbol{x},\dot{\boldsymbol{x}})\dot{\boldsymbol{x}}_d - \boldsymbol{D}_d\dot{\tilde{\boldsymbol{x}}} - \boldsymbol{K}_d\tilde{\boldsymbol{x}}. \quad (4)$$

Transforming $\boldsymbol{F}_\tau = {\boldsymbol{J}_e}^{-T}\boldsymbol{\tau} + {\boldsymbol{J}_e}^{-T}\boldsymbol{J}_{st}^T\boldsymbol{F}_{st} \in \mathbb{R}^6$ in (2) into the joint space, the compliance controller input is as follows:

$$\underbrace{\begin{bmatrix}\boldsymbol{0}_{6\times1}\\ \boldsymbol{\tau}_l\\ \boldsymbol{\tau}_a\end{bmatrix}}_{\boldsymbol{\tau}} + \underbrace{\begin{bmatrix}\boldsymbol{J}_{st,b}^T\\ \boldsymbol{J}_{st,l}^T\\ \boldsymbol{0}_{n_a\times3n_c}^T\end{bmatrix}}_{\boldsymbol{J}_{st}^T}\boldsymbol{F}_{st} = \underbrace{\begin{bmatrix}\boldsymbol{J}_{e,b}^T\\ \boldsymbol{0}_{n_l\times6}^T\\ \boldsymbol{J}_{e,a}^T\end{bmatrix}}_{\boldsymbol{J}_e^T}\boldsymbol{F}_\tau. \quad (5)$$

Since the contribution of the legs' torques $\boldsymbol{\tau}_l$ in the (5) is not significant, one can extract the top six rows and the bottom n_a rows. Then, the compliance controller input can be decoupled as:

$$\begin{bmatrix}\boldsymbol{J}_{st,b}^T\boldsymbol{F}_{st}\\ \boldsymbol{\tau}_a\end{bmatrix} = \begin{bmatrix}\boldsymbol{J}_{e,b}^T\\ \boldsymbol{J}_{e,a}^T\end{bmatrix}\boldsymbol{F}_\tau \quad (6)$$

where $\boldsymbol{J}_{st,b}^T\boldsymbol{F}_{st}$ controls the locomotion of the base, and $\boldsymbol{\tau}_a$ controls the each joint of the manipulator. Through (6), the quadruped manipulator is decomposed into $6 + n_a$ independent systems.

Let us define the variables $\boldsymbol{\tau}_o = \begin{bmatrix}\boldsymbol{F}_{st}^T\boldsymbol{J}_{st,b} & \boldsymbol{\tau}_a^T\end{bmatrix}^T$ and $\boldsymbol{\tau}_o^d = \begin{bmatrix}\boldsymbol{J}_{e,b} & \boldsymbol{J}_{e,a}\end{bmatrix}^T\boldsymbol{F}_\tau$ from (6). To simultaneously satisfy the torque limits and stability requirements of legged robot as in (3b) and (3c), let us extend the admittance scheme in [17]:

$$\boldsymbol{\tau}_o^f + \boldsymbol{\tau}_o^d - \mathcal{N}_{\boldsymbol{\mathcal{F}}}(\boldsymbol{\tau}_o) \in \boldsymbol{M}_o\left(\ddot{\boldsymbol{q}}_s - \ddot{\boldsymbol{q}}_0\right) + \quad (7a)$$

$$\boldsymbol{D}_o\left(\dot{\boldsymbol{q}}_s - \dot{\boldsymbol{q}}_0\right) + \boldsymbol{K}_o\left(\boldsymbol{q}_s - \boldsymbol{q}_0\right), \dot{\boldsymbol{a}} = \boldsymbol{q}_s - \boldsymbol{q} \quad (7b)$$

$$\boldsymbol{\tau}_o = \boldsymbol{M}_s\ddot{\boldsymbol{q}}_s + \boldsymbol{K}_s\left(\boldsymbol{q}_s - \boldsymbol{q}\right) + \boldsymbol{D}_s\left(\dot{\boldsymbol{q}}_s - \dot{\boldsymbol{q}}\right) + \boldsymbol{L}_s\boldsymbol{a} \quad (7c)$$

where $\boldsymbol{q}_s \in \mathbb{R}^{6+n_a}$ is the position of proxy, $\boldsymbol{q}_0 \in \mathbb{R}^{6+n_a}$ is the desired position defined by the operators (Sec. II-B), $\boldsymbol{q} \in \mathbb{R}^{6+n_a}$ is the measured position of the controlled object, $\boldsymbol{\tau}_o^f$ is the measured or estimated augment torque of $\boldsymbol{\tau}_o$. The inertia $\boldsymbol{M}_o \in \mathbb{R}^{(6+n_a)\times(6+n_a)}$, viscosity $\boldsymbol{B}_o \in \mathbb{R}^{(6+n_a)\times(6+n_a)}$, and stiffness $\boldsymbol{K}_o \in \mathbb{R}^{(6+n_a)\times(6+n_a)}$ build the dynamics of the proxy, the notation $\mathcal{N}_{\boldsymbol{\mathcal{F}}}(\boldsymbol{\tau}_o)$ represents the normal cone of the set $\boldsymbol{\mathcal{F}}$ at $\boldsymbol{\tau}_o$, which can be written as: $\mathcal{N}_{\boldsymbol{\mathcal{F}}}(\boldsymbol{\tau}_o) \triangleq \{\boldsymbol{z} \mid \boldsymbol{z}^T(\boldsymbol{\tau}_o^* - \boldsymbol{\tau}_o) \le \boldsymbol{0}, \forall\boldsymbol{\tau}_o^* \in \boldsymbol{\mathcal{F}}\}$ with the set $\boldsymbol{\mathcal{F}} = [F_1, F_2]^{6+n_a}$ being the limit. The equation (7b) represents a PID position controller with a feedforward of the desired acceleration. The coefficients $\boldsymbol{K}_s$, $\boldsymbol{D}_s$, and $\boldsymbol{L}_s$ are proportional, derivative, and integral gains, respectively.

Different from the work [17], the set $\boldsymbol{\mathcal{F}}$ in the nonmsooth operator $\mathcal{N}_{\boldsymbol{\mathcal{F}}}(\boldsymbol{\tau}_o)$ not only considers the torque saturation levels in (3b), that is, torque limit $[\boldsymbol{\tau}_{\min}, \boldsymbol{\tau}_{\max}]$ of each joint of the manipulator, but also the friction cone (3c) of legged base, that is, the square pyramid to approximate the friction cone with linear constraints [22]. Therefore, $\boldsymbol{\mathcal{F}} = [\boldsymbol{f}_{\min}, \boldsymbol{f}_{\max}]$ for the base's locomotion is defined as

$$\boldsymbol{f}_{\max} = [\mu f_z, \mu f_z, f_{\max}, f_{\max}, f_{\max}, f_{\max}]^T \quad (8a)$$

$$\boldsymbol{f}_{\min} = [-\mu f_z, -\mu f_z, f_{\min}, f_{\min}, f_{\min}, f_{\min}]^T \quad (8b)$$

where μ is the friction coefficient and f_z is the z-component of $\boldsymbol{J}_{st,b}^T\boldsymbol{F}_{st}$. Therefore the augment variable $\boldsymbol{\tau}_o$ is bounded by the $\mathcal{N}_{\boldsymbol{\mathcal{F}}}(\boldsymbol{\tau}_o)$, subjected to (3b) and (3c).

The equation (7) constitute a pair of simultaneous equations with two unknowns $\boldsymbol{\tau}_o$ and $\ddot{\boldsymbol{q}}_s$. When the $\boldsymbol{\tau}_o$ is within the limit, i.e., $\boldsymbol{\tau}_o \in \boldsymbol{\mathcal{F}}$, the equation (9) is equivalent to the conventional admittance scheme, which tracks the commanded augment torque $\boldsymbol{\tau}_o^d$ by tracking the proxy states $\ddot{\boldsymbol{q}}_s$. When the $\boldsymbol{\tau}_o$ is saturated caused by the external force $\boldsymbol{F}_e$ or $\boldsymbol{F}_b$, i.e., $\boldsymbol{\tau}_o \notin \boldsymbol{\mathcal{F}}$, the set-valued algebraic feedback will force the deviation between the proxy position $\boldsymbol{q}_s$ and the actual position $\boldsymbol{q}$ to be limited. By doing so, the

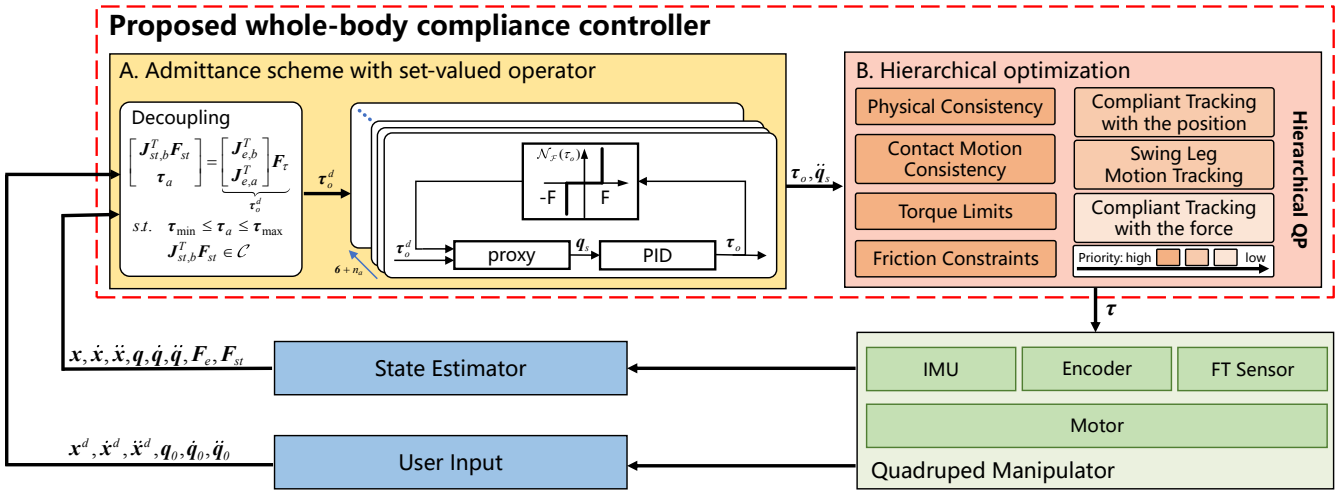

Fig. 3. The block diagram of the proposed method for the quadruped manipulator whole-body compliance controller with actuation saturation. Firstly, the compliance controller input is decoupled as the manipulation $\boldsymbol{\tau}_a$ and the locomotion $\boldsymbol{J}_{st,b}^T \boldsymbol{F}_{st}$ based on the operator's input and the state estimator. Then, an admittance scheme with a set-valued operator generates proxy states $\ddot{\boldsymbol{q}}_s$ and $\boldsymbol{\tau}_o$ based on commands $\boldsymbol{\tau}_o^d$, eliminating unsafe behaviors caused by actuation saturation. Finally, with the proxy states $\ddot{\boldsymbol{q}}_s$ and $\boldsymbol{\tau}_o$, an optimization problem is formulated by Hierarchical Quadratic Programming (HQP) to impose the admittance scheme's output for the robot while satisfying physical consistency.

method tracks the commanded augment torque $\boldsymbol{\tau}_o^d$ by the proxy rather than tracking it directly. It can avoid the huge deviation between $\boldsymbol{\tau}_o$ and $\boldsymbol{\tau}_o^d$ when the actuation saturation occurs. Thus, it mitigates safety issues like oscillations, and overshooting that typically arise when the controller tries to eliminate the huge deviation with actuation saturation.

With the help of the set-valued operator in (7), the compliance property of the admittance scheme is adjusted based on $\boldsymbol{\tau_o}$. Specifically, when $\boldsymbol{\tau_o}$ is within the limit, the compliance property approximates the desired Cartesian impedance defined in (4). When $\boldsymbol{\tau_o}$ reaches the limit, the compliance property is kept as the low impedance to yield to external forces or recover from a huge deviation between commands $\boldsymbol{\tau_o^d}$ and the robot.

To discretize (7), the equivalently transforming relation $\boldsymbol{z} + \mathcal{N}_{\boldsymbol{\mathcal{F}}}(\boldsymbol{z}) \ni \boldsymbol{y} \Leftrightarrow \boldsymbol{z} = \text{proj}_{\boldsymbol{\mathcal{F}}}(\boldsymbol{y})$ is used [17], where $\text{proj}_{\boldsymbol{\mathcal{F}}}(\boldsymbol{y})$ is the saturation function that projects $\boldsymbol{y}$ onto the set $\boldsymbol{\mathcal{F}}$ and can be written as: $\text{proj}_{\boldsymbol{\mathcal{F}}}(\boldsymbol{y}) := \text{argmin}_{\boldsymbol{\xi} \in \boldsymbol{\mathcal{F}}} (\boldsymbol{\xi} - \boldsymbol{y})^2$. Therefore, (7) can be discretized using implicit Euler discretization [23] as follows:

$$\boldsymbol{q}_s^*(k) := \boldsymbol{q}_s(k-1) + T\boldsymbol{u}_s^*(k) \tag{9a}$$

$$\boldsymbol{\phi}_b(k) := \frac{\boldsymbol{D}_s\left(\boldsymbol{q}_s(k-1) - \boldsymbol{q}(k-1)\right)}{T} - \boldsymbol{L}_s\boldsymbol{a}(k-1) \tag{9b}$$

$$\boldsymbol{\phi}_a(k) := \boldsymbol{M}_s \frac{\boldsymbol{q}(k) - \boldsymbol{q}_s(k-1) - T\boldsymbol{u}_s(k-1)}{T^2} \tag{9c}$$

$$\boldsymbol{q}^*(k) := \boldsymbol{q}(k) + (\boldsymbol{\phi}_b(k) - \boldsymbol{\phi}_a(k))(\hat{\boldsymbol{K}} + \boldsymbol{M}/T^2)^{-1} \tag{9d}$$

$$\boldsymbol{\tau}_o^*(k) := \boldsymbol{S}_2\boldsymbol{S}_1^{-1}\boldsymbol{q}_s^*(k) - \boldsymbol{S}_2\boldsymbol{q}^*(k) \tag{9e}$$

$$\boldsymbol{\tau}_o(k) := \text{proj}_{\boldsymbol{\mathcal{F}}}\left(\boldsymbol{\tau}_o^*(k)\right) \tag{9f}$$

where T is time stepping size, $k \in \mathbb{N}_0$ is the index of time stepping, $\hat{\boldsymbol{K}} := \boldsymbol{K}_s + \boldsymbol{D}_s/T + T\boldsymbol{L}_s$, $\boldsymbol{S}_1 := \boldsymbol{E} + T^2\boldsymbol{K}_o(\boldsymbol{M}_o + T\boldsymbol{D}_o)^{-1}$, $\boldsymbol{S}_2 := \hat{\boldsymbol{K}} + \boldsymbol{M}_s/T^2$, $\boldsymbol{S}_3 := \boldsymbol{M}_o + T\boldsymbol{D}_o$ are the gains, and $\boldsymbol{\tau}_o(k)$ is the output torque of the admittance scheme. The set-valuedness in the original equation (7) is implicitly preserved in the algorithm (9). The intermediate variables $\boldsymbol{q}_s(k), \boldsymbol{u}_s(k)$ and $\boldsymbol{a}(k)$ are updated as follows:

$$\boldsymbol{q}_0^*(k) = \boldsymbol{M}_o\ddot{\boldsymbol{q}}_0(k) + \boldsymbol{D}_o\dot{\boldsymbol{q}}_0(k) + \boldsymbol{K}_o\boldsymbol{q}_0(k) + \boldsymbol{\tau}_o^f(k) \tag{10a}$$

$$\boldsymbol{u}_s^*(k) := (\boldsymbol{M}_o\boldsymbol{u}_s(k-1) + T(\boldsymbol{q}_0^*(k) - \boldsymbol{\tau}_o^d(k)))\boldsymbol{S}_3^{-1} \tag{10b}$$

$$\boldsymbol{q}_s(k) := \boldsymbol{q}^*(k) + \boldsymbol{\tau}(k)(\hat{\boldsymbol{K}} + \boldsymbol{M}/T^2)^{-1} \tag{10c}$$

$$\boldsymbol{u}_s(k) := \left(\boldsymbol{q}_s(k) - \boldsymbol{q}_s(k-1)\right)/T \tag{10d}$$

$$\boldsymbol{a}(k) := \boldsymbol{a}(k-1) + T\left(\boldsymbol{q}_s(k) - \boldsymbol{q}(\boldsymbol{k})\right). \tag{10e}$$

TABLE I
THE TASKS USED IN THE WBC. EACH TASK IS ASSOCIATED WITH A PRIORITY (1 IS THE HIGHEST).

Priority	Task
1	Physical Consistency
	Contact Motion Consistency
	Torque Limits
	Friction Constraints
2	Compliant Tracking with the position
	Swing Leg Motion Tracking
3	Compliant Tracking with the force

B. Hierarchical optimization

The PID position controller with feedforward of desired acceleration, calculated using equation (7), may not perform optimally for nonlinear systems like the quadruped manipulator. To maintain the compliance properties of the admittance scheme, avoid unsafe behaviors caused by actuation saturation, and ensure physical consistency, we solve a hierarchical optimization problem based on HQP [24] to find optimal actuators' torques. The solver finds solutions for lower-priority tasks in the null space of higher-priority tasks without conflicting with them. Tab. I lists prioritized tasks used in the hierarchical optimization problem where smaller numbers indicate higher priorities.

Let $\boldsymbol{\xi} = [\dot{\boldsymbol{v}}^T, \boldsymbol{F}_{st}^T]^T \in \mathbb{R}^{6+n_l+n_a+3n_c}$ be the optimization variable. The solver searches for the optimal $\boldsymbol{\xi}_d$ in tasks and then calculates the optimal actuators' torques.

1) Compliance Tracking: The compliance tracking task realizes the admittance scheme's output and is divided into two sub-tasks. One is compliance tracking with the position, which controls the robot to track the proxy state $\left[\boldsymbol{q}_s^T, \dot{\boldsymbol{q}}_s^T, \ddot{\boldsymbol{q}}_s^T\right]^T$ directly with high priority. Therefore, we have:

$$\begin{bmatrix} \mathbb{I}_{6\times 6} & \mathbf{0}_{n_l\times n_l} & \mathbb{I}_{n_a\times n_a} & \mathbf{0}_{3n_c\times 3n_c} \end{bmatrix} \boldsymbol{\xi} = \ddot{\boldsymbol{q}}_s + \boldsymbol{M}_s^{-1}\boldsymbol{D}_s\left(\dot{\boldsymbol{q}}_s - \dot{\boldsymbol{q}}\right) + \boldsymbol{M}_s^{-1}\boldsymbol{K}_s\left(\boldsymbol{q}_s - \boldsymbol{q}\right). \tag{11}$$

The other is compliance tracking with the force, which controls the robot to track $\boldsymbol{\tau}_o$ with low priority. Therefore, we have:

$$\begin{bmatrix} \mathbf{0} & \boldsymbol{J}_{st,b}^T \end{bmatrix} \boldsymbol{\xi}_d = \begin{bmatrix} \mathbb{I}_{6\times 6} & \mathbf{0}_{n_a\times n_a} \end{bmatrix} \boldsymbol{\tau}_o \tag{12a}$$

$$\begin{bmatrix} \boldsymbol{M}_{ab} & \boldsymbol{M}_{al} & \boldsymbol{M}_a & -\mathbf{0}_{n_a\times 3n_c}^T \end{bmatrix} \boldsymbol{\xi} = -\boldsymbol{n}_a + \boldsymbol{J}_{e,a}^T\boldsymbol{F}_e + \begin{bmatrix} \mathbf{0}_{6\times 6} & \mathbb{I}_{n_a\times n_a} \end{bmatrix} \boldsymbol{\tau}_o. \tag{12b}$$

The solver prioritizes tracking proxy state $\left[\boldsymbol{q}_s^T, \dot{\boldsymbol{q}}_s^T, \ddot{\boldsymbol{q}}_s^T\right]^T$ over force $\boldsymbol{\tau}_o$ with varying priorities. As a result, if $\boldsymbol{\tau}_o$ violates physical consistency, it will be relaxed to ensure that the compliance properties of the admittance scheme can be realized.

2) Physical Consistency: The dynamics of the quadruped manipulator in (1) sets a relationship between contact forces $\boldsymbol{F}_{st}$ and motion $\dot{\boldsymbol{v}}$. To enforce physical consistency constraint in the relationship, the floating-base dynamics from the top six rows of (1) is used as:

$$[\boldsymbol{M}_b\ \boldsymbol{M}_{bl}\ \boldsymbol{M}_{ba}\ -\boldsymbol{J}_{st,b}^T]\boldsymbol{\xi} = -\boldsymbol{n}_b + \boldsymbol{J}_{e,b}^T\boldsymbol{F}_e. \tag{13}$$

3) Contact Motion Consistency: The solution found by the solver should ensure the null accelerations of stance legs at the contact points. Therefore, we design:

$$[\boldsymbol{J}_{st}\ \mathbf{0}_{3n_c\times 3n_c}]\,\boldsymbol{\xi} = -\dot{\boldsymbol{J}}_{st}\boldsymbol{v} \tag{14}$$

for each stance leg.

4) Torque Limits: To avoid violation of actuator's torque limits, we design $\underline{\boldsymbol{d}}_\tau < \boldsymbol{C}_\tau\boldsymbol{\xi} < \overline{\boldsymbol{d}}_\tau$, with

$$\underline{\boldsymbol{d}}_\tau = \begin{bmatrix} -\boldsymbol{n}_l + \boldsymbol{\tau}_{l,\min} \\ -\boldsymbol{n}_a + \boldsymbol{J}_{e,a}^T\boldsymbol{F}_e + \boldsymbol{\tau}_{a,\min} \end{bmatrix} \tag{15a}$$

$$\boldsymbol{C}_\tau = \begin{bmatrix} \boldsymbol{M}_{lb} & \boldsymbol{M}_l & \boldsymbol{M}_{la} & -\boldsymbol{J}_{st,l}^T \\ \boldsymbol{M}_{ab} & \boldsymbol{M}_{al} & \boldsymbol{M}_a & -\mathbf{0}_{n_a\times 3n_c} \end{bmatrix} \tag{15b}$$

$$\overline{\boldsymbol{d}}_\tau = \begin{bmatrix} -\boldsymbol{n}_l + \boldsymbol{\tau}_{l,\max} \\ -\boldsymbol{n}_a + \boldsymbol{J}_{e,a}^T\boldsymbol{F}_e + \boldsymbol{\tau}_{a,\max} \end{bmatrix}. \tag{15c}$$

5) Friction Constraints: To avoid slipping, contact forces should be constrained to stay in the friction cone. We approximate friction cones with square pyramids to express them with linear constraints: $\left[\mathbf{0}_{5n_c\times(6+n_l+n_a)}\ \boldsymbol{F}_{fr}\right]\boldsymbol{\xi} < \mathbf{0}$ with

$$\boldsymbol{F}_{fr} = \begin{bmatrix} \boldsymbol{F}_{lc} & \cdots & 0 \\ \vdots & \ddots & \vdots \\ 0 & \cdots & \boldsymbol{F}_{lc} \end{bmatrix}, \boldsymbol{F}_{lc} = \begin{bmatrix} 0 & 0 & -1 \\ 1 & 0 & -\mu \\ -1 & 0 & -\mu \\ 0 & 1 & -\mu \\ 0 & -1 & -\mu \end{bmatrix}.$$

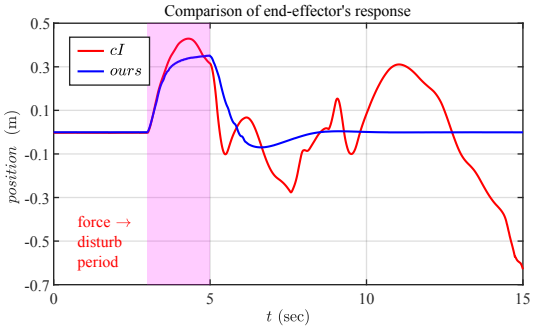

Fig. 4. Motion response along the x-axis for the manipulator's end-effector caused by controllers when an external force of $50N$ is applied to the end-effector at the third second for 2 seconds. The red line is the response caused by the **cI**, denoting the approach consisting of an impedance controller and WBC [11]. The blue line is the response caused by our approach.

6) Swing Leg Motion Tracking: Each swing leg is built into this task to track the pre-defined desired swing trajectory [25]. The task is defined as

$$\begin{bmatrix} \boldsymbol{J}_{st,b} & \boldsymbol{J}_{st,l} & \mathbf{0} \end{bmatrix} \boldsymbol{\xi} = \ddot{\boldsymbol{\phi}}^d + k_D\dot{\tilde{\boldsymbol{\phi}}} + k_P\tilde{\boldsymbol{\phi}} - \begin{bmatrix} \dot{\boldsymbol{J}}_{st,b} & \dot{\boldsymbol{J}}_{st,l} & \mathbf{0} \end{bmatrix} \boldsymbol{v} \tag{16}$$

where $\tilde{\boldsymbol{\phi}}$ and $\dot{\tilde{\boldsymbol{\phi}}} \in \mathbb{R}^3$ are the position and linear velocity error, respectively, and $\ddot{\boldsymbol{\phi}}^d \in \mathbb{R}^3$ is the desired linear acceleration of the pre-defined swing trajectory, k_P and $k_D \in \mathbb{R}$ are control gains for the position and linear velocity, respectively.

7) Torque Computation: With the optimal accelerations and contact forces $\boldsymbol{\xi}_d$ solved by optimization, the optimal torques for the legs and the arm can be computed as:

$$\begin{bmatrix} \boldsymbol{\tau}_l \\ \boldsymbol{\tau}_a \end{bmatrix} = \begin{bmatrix} \boldsymbol{M}_{lb} & \boldsymbol{M}_l & \boldsymbol{M}_{la} & -\boldsymbol{J}_{st,l}^T \\ \boldsymbol{M}_{ab} & \boldsymbol{M}_{al} & \boldsymbol{M}_a & -\mathbf{0}_{n_a\times 3n_c} \end{bmatrix} \boldsymbol{\xi}_d + \begin{bmatrix} \boldsymbol{n}_l \\ \boldsymbol{n}_a \end{bmatrix} - \begin{bmatrix} \mathbf{0}_{n_l\times 6} \\ \boldsymbol{J}_{e,a}^T \end{bmatrix} \boldsymbol{F}_e. \tag{17}$$

IV. EXPERIMENTS

The quadruped manipulator for validating the proposed methods consists of a torque-controllable quadruped robot, Aliengo [26], a 6-DOF manipulator, Kinova gen2 [27], and a force/torque sensor from SRI [28]. Therefore, the robot has $n_l = 12$, $n_a = 6$, with twelve and six DoFs describing legs and the arm. The full control framework is depicted in Fig. 3, and all of the modules run on the user's computer (Intel Core i7-11700F@2.50GHz). The proposed approach was validated in a simulator developed in the Gazebo environment [29]. The admittance scheme with set-valued operator (Sec. III-A) and hierarchical optimization (Sec. III-B) run at a frequency of approximately 1000Hz. The hierarchical optimization (Sec. III-B) based on the HQP is solved by QPOASES [30]. The state estimator used in the controller is based on the work in [31] fusing measurements from the motors' encodes and IMU. We use Pinocchio [32] to generate the model of the kinematics and dynamics of the robot. For the sake of space, experiments present the

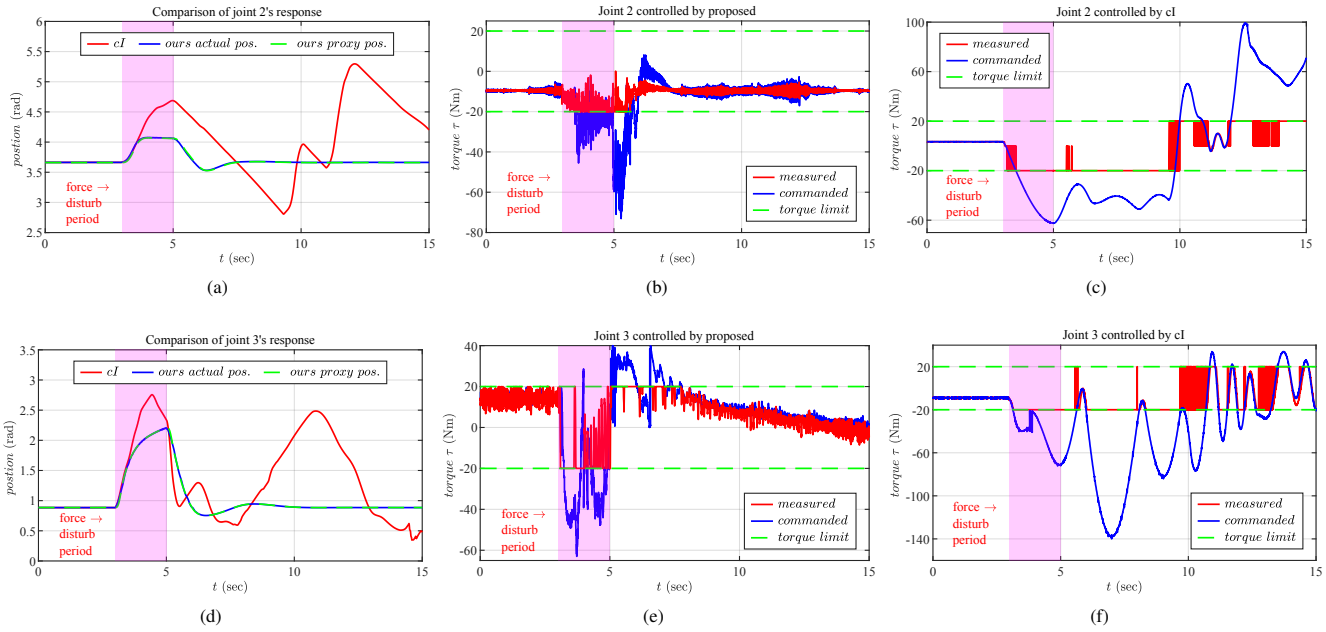

Fig. 5. Simulation results of whole-body compliance control with an external force of $50N$ applied to the manipulator's end-effector at the third second for 2 seconds. The results only show saturated joints, which are the second and third joints of the manipulator (i.e., joint2 and joint3). (a) and (d) are the motion responses of joint2 and joint3, respectively. The red solid line is the response caused by the **cI** [11]. The blue solid line and the green dotted line are the actual and proxy responses caused by our approach, respectively. (b) and (e) are torque results caused by our approach. (c) and (f) are torque results caused by the **cI** [11]. The red solid line is the time history of the measured torque, the blue solid line is the time history of the commanded torque, and the green dotted line is the torque limit with $20N \cdot m$.

manipulator's end-effector compliance for only x cartesian dimensions, which is the most relevant one for stability in legged systems. The other directions of the manipulator's end-effector are fixed. For the sake of clarity, the plots only show the results of joints that are saturated.

The parameters were chosen as $K_{d_x} = 2000$ and $D_{d_x} = 20$ in (4), where the subscript x stands for x-component. Let us set $\boldsymbol{M}_{o_a} = \text{diag}(10)^{n_a}$, $\boldsymbol{D}_{o_a} = \text{diag}(30)^{n_a}$, $\boldsymbol{K}_{o_a} = \text{diag}(300)^{n_a}$, $\boldsymbol{M}_{o_a} = \text{diag}(5)^{n_a}$, $\boldsymbol{K}_{o_a} = \text{diag}(2000)^{n_a}$, $\boldsymbol{D}_{o_a} = \text{diag}(10)$, $\boldsymbol{L}_{o_a} = \text{diag}(5)^{n_a}$ for the manipulator's joints and $\boldsymbol{M}_{o_b} = \text{diag}(10)^6$, $\boldsymbol{D}_{o_b} = \text{diag}(700)^6$, $\boldsymbol{K}_{o_b} = \text{diag}(500)^6$, $\boldsymbol{M}_{s_b} = \text{diag}(5)^6$, $\boldsymbol{K}_{s_b} = \text{diag}(20000)^6$, $\boldsymbol{D}_{s_b} = \text{diag}(400)^6$, $\boldsymbol{L}_{s_b} = \text{diag}(0)^6$ for the base in (7), where the subscripts a and b stand for the arm and base, respectively. The actuators' torque limit was chosen as $\tau_{max} = -\tau_{min} = 20N \cdot m$ for each manipulator's joint, and the friction coefficient was chosen as $\mu = 0.1$. The timestep size was set as $T = 0.001s$ in (7). The parameters of swing leg motion tracking in the hierarchical optimization (16) were chosen as $k_D = 37$, $k_P = 350$.

For comparisons, we used the **cI**, an impedance controller combined with the WBC proposed in [11]. The project has been released on GitHub[2], and the video submission[3] supports all of the examples discussed in this paper.

A. Force on the End-Effector

In the 1st set of experiments, an external force of $50N$ was applied to the manipulator's end-effector along the x-axis at the third second for 2s, i.e., $\boldsymbol{F}_e = [50, 0, 0, 0, 0, 0]^T$ N. The results are shown in Fig. 4 and Fig. 5, where the second and third joints of the manipulator (i.e., joint2 and joint3) are saturated.

From Fig. 4, when the external force was applied, the manipulator's end-effector was pulled away from the desired position. After the external force was removed at the fifth second, the motion produced by **cI** was overshooting and oscillatory, whereas that produced by our approach was rather smooth and monotonic. The reason is that our approach can eliminate unsafe behaviors caused by actuation saturation, which will be explained in detail below. From Fig. 5, when the external force was applied, commanded torques of joint2 and joint3 generated by (4) far exceeded the torque limit and were outside the robot's range of motion. It led to the actuation saturation and the separation between the commanded torques and the output torques of the controller. **cI** tried to eliminate huge deviations directly resulting in snapping-back motions of joints with overshoots and oscillations after removing the external force. Eventually, **cI** made the motion response of the manipulator's end-effector diverge, and the robot became unstable. However, there was no unsafe behavior with our approach. This is because our approach tracks the proxy in (7) rather than tracking commanded torques directly like **cI**. From Fig. 5a and Fig. 5d, when the external force was applied, leading to the actuation saturation, the proxy followed the actual position of joints rather than being controlled by commanded torques. The compliance property of the admittance scheme kept the low impedance to yield to the external force. Thus,

[2]Available at https://github.com/skywoodsz/qm_control
[3]Available at `https://youtu.be/gK7PCxNsuZ8`

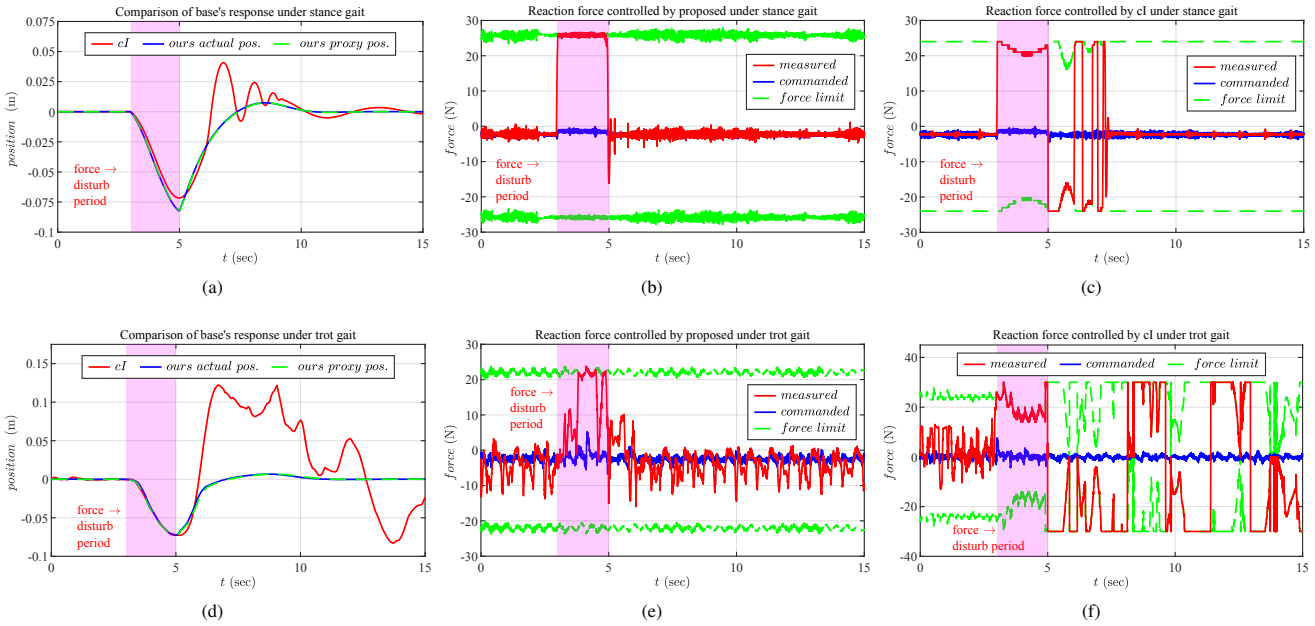

Fig. 6. Simulation results of whole-body compliance control with an external force of $50N$ applied to the base at the third second for 2 seconds. (a) and (d) are motion responses along the x-axis for the base under stance and trot gait, respectively. The red solid line is the response caused by the **cI** [11]. The blue solid line and the green dotted line are the actual and proxy responses caused by our approach, respectively. (b) and (e) are the x-component of reaction forces $\boldsymbol{J}_{st,b}^{T}\boldsymbol{F}_{st}$ caused by our approach. (c) and (f) are the x-component of reaction forces $\boldsymbol{J}_{st,b}^{T}\boldsymbol{F}_{st}$ caused by **cI** [11]. The red solid line is the time history of the measured force, the blue solid line is the time history of the commanded force, and the green dotted line is the time history of the force limit subject to the friction cone with friction coefficient $\mu = 0.1$.

when the external force was removed, there was no huge separation between the proxy and the actual position, avoiding oscillations and overshoots. The compliance property of the admittance scheme kept the low impedance to recovery from a huge deviation between command torques and output torques produced by our approach. In the non-saturation case, the proxy tracks commanded torques by the admittance scheme, and the compliance property of the admittance scheme approximated the high Cartesian impedance defined by the operator, which can be seen in Fig. 5b and Fig. 5e. Finally, the end-effector smoothly reached the desired position, and the robot remained stable.

B. Force on the Base

In the 2nd set of experiments, an external force of $50N$ was applied to the base at the third second for 2 seconds, i.e., $\boldsymbol{F}_b = [50, 0, 0, 0, 0, 0]^T\ N$, which can not be measured. To illustrate the method's effectiveness, the external force was applied to the base under the stance and trot gait, respectively.

The results of the base under the stance gait are shown in Fig. 6a, Fig. 6b, and Fig. 6c. From Fig. 6b and Fig. 6c, since the external force can not be obtained, the commanded force generated by (4) had almost no change. Although the command forces did not exceed limits and were within the range of robot's motion, output forces were pushed to the saturation to resist the external force disturbance. Therefore, this led to a huge separation between commanded and output forces. After the external force was removed at the fifth second, the huge separation made the output force produced by **cI** repeated transitions between negative and positive saturation. This further caused snapping-back motions of the base with overshoots and oscillations, which can be seen in Fig. 6a. However, the results produced by our approach were different. From Fig. 6a and Fig. 6b, when the external force was applied to the base, the output force was bounded, and the proxy attached to the actual position of the base. After removing the external force, there was no separation between the proxy and the actual position. Thus, the output force tracked the commanded force smoothly and monotonically, avoiding repeated transitions between negative and positive saturation. Finally, the base smoothly reached the desired position, avoiding oscillations and overshoots.

Compared with the robot under the stance gait, it would be more difficult to be stabilized when the robot is under the trot gait. The results of the base under the trot gait are shown in Fig. 6d, Fig. 6e, and Fig. 6f. From Fig. 6e, and Fig. 6f, when the external force was applied to the base, output forces produced by **cI** and our approach reached the saturation, and commanded forces did not change. However, with the huge deviation between commanded forces and output forces, **cI** made the output forces repeat transitions between negative and positive saturation, resulting in the robot's overshooting and oscillatory motion. Finally, **cI** pushed the robot to be unstable. As for our approach, the base smoothly and monotonically reached the desired position after removing the external force. The reason is also that the proxy prevented large deviation caused by actuation saturation, avoiding unsafe behaviors such as slip, overshoots and oscillations.

V. CONCLUSIONS

This paper presents a whole-body compliance controller for a quadruped manipulator that improves overall stability under actuation saturation. The controller considers actuator torque limits and friction cone of the ground reaction force of the legged body as actuation saturation, allowing the robot to be stabilized even when force sensors cannot measure external forces. By adjusting the compliance property of the admittance scheme within set-valued operator constraints on actuation torques and ground reaction forces, the controller avoids unsafe behaviors caused by actuation saturation such as slips, oscillations, and overshoots. Hierarchical optimization is used to maintain the compliance property of the admittance scheme while maintaining physical consistency.

Experimental results demonstrate that this method robustly eliminates the effects of actuation saturation during interactions with large external force disturbances. However, in non-saturated cases, the method can only approximate the desired impedance. Future work may address this limitation by extending the proposed method's application to build a whole-body admittance controller with actuation saturation.

REFERENCES

[1] P. Arm, G. Waibel, J. Preisig, T. Tuna, R. Zhou, V. Bickel, G. Ligeza, T. Miki, F. Kehl, H. Kolvenbach *et al.*, "Scientific exploration of challenging planetary analog environments with a team of legged robots," *Science robotics*, vol. 8, no. 80, p. eade9548, 2023.

[2] C. D. Bellicoso, K. Krämer, M. Stäuble, D. Sako, F. Jenelten, M. Bjelonic, and M. Hutter, "Alma-articulated locomotion and manipulation for a torque-controllable robot," in *2019 International conference on robotics and automation (ICRA)*. IEEE, 2019, pp. 8477–8483.

[3] P. Ewen, J.-P. Sleiman, Y. Chen, W.-C. Lu, M. Hutter, and R. Vasudevan, "Generating continuous motion and force plans in real-time for legged mobile manipulation," in *2021 IEEE International Conference on Robotics and Automation (ICRA)*. IEEE, 2021, pp. 4933–4939.

[4] M. H. Raibert, *Legged robots that balance*. MIT press, 1986.

[5] F. Angelini, G. Xin, W. J. Wolfslag, C. Tiseo, M. Mistry, M. Garabini, A. Bicchi, and S. Vijayakumar, "Online optimal impedance planning for legged robots," in *2019 IEEE/RSJ International Conference on Intelligent Robots and Systems (IROS)*. IEEE, 2019, pp. 6028–6035.

[6] S. Caron, A. Kheddar, and O. Tempier, "Stair climbing stabilization of the hrp-4 humanoid robot using whole-body admittance control," in *2019 International conference on robotics and automation (ICRA)*. IEEE, 2019, pp. 277–283.

[7] B. Ugurlu, I. Havoutis, C. Semini, and D. G. Caldwell, "Dynamic trot-walking with the hydraulic quadruped robot—hyq: Analytical trajectory generation and active compliance control," in *2013 IEEE/RSJ International Conference on Intelligent Robots and Systems*. IEEE, 2013, pp. 6044–6051.

[8] R. Parosi, M. Risiglione, D. G. Caldwell, C. Semini, and V. Barasuol, "Kinematically-decoupled impedance control for fast object visual servoing and grasping on quadruped manipulators," in *2023 IEEE/RSJ International Conference on Intelligent Robots and Systems (IROS)*. IEEE, 2023, pp. 1–8.

[9] M. J. Pollayil, F. Angelini, G. Xin, M. Mistry, S. Vijayakumar, A. Bicchi, and M. Garabini, "Choosing stiffness and damping for optimal impedance planning," *IEEE Transactions on Robotics*, vol. 39, no. 2, pp. 1281–1300, 2022.

[10] C. Ott, R. Mukherjee, and Y. Nakamura, "Unified impedance and admittance control," in *2010 IEEE international conference on robotics and automation*. IEEE, 2010, pp. 554–561.

[11] M. Risiglione, V. Barasuol, D. G. Caldwell, and C. Semini, "A whole-body controller based on a simplified template for rendering impedances in quadruped manipulators," in *2022 IEEE/RSJ International Conference on Intelligent Robots and Systems (IROS)*. IEEE, 2022, pp. 9620–9627.

[12] E. M. Hoffman, A. Laurenzi, L. Muratore, N. G. Tsagarakis, and D. G. Caldwell, "Multi-priority cartesian impedance control based on quadratic programming optimization," in *2018 IEEE International Conference on Robotics and Automation (ICRA)*. IEEE, 2018, pp. 309–315.

[13] S. Singh, R. P. Russell, and P. M. Wensing, "Analytical second-order partial derivatives of rigid-body inverse dynamics," in *2022 IEEE/RSJ International Conference on Intelligent Robots and Systems (IROS)*. IEEE, 2022, pp. 11 781–11 788.

[14] R. Kikuuwe and H. Fujimoto, "Proxy-based sliding mode control for accurate and safe position control," in *Proceedings 2006 IEEE International Conference on Robotics and Automation, 2006. ICRA 2006.* IEEE, 2006, pp. 25–30.

[15] R. Kikuuwe, S. Yasukouchi, H. Fujimoto, and M. Yamamoto, "Proxy-based sliding mode control: A safer extension of pid position control," *IEEE Transactions on Robotics*, vol. 26, no. 4, pp. 670–683, 2010.

[16] R. Kikuuwe, "A sliding-mode-like position controller for admittance control with bounded actuator force," *IEEE/ASME Transactions On Mechatronics*, vol. 19, no. 5, pp. 1489–1500, 2013.

[17] R. Kikuuwe, "Torque-bounded admittance control realized by a set-valued algebraic feedback," *IEEE Transactions on Robotics*, vol. 35, no. 5, pp. 1136–1149, 2019.

[18] X. Yuan, Y. Ding, X. Xiong, and Y. Lou, "Torque-bounded admittance control with implicit euler realization of set-valued operators," *IEEE/ASME Transactions on Mechatronics*, 2023.

[19] T. Zhang, S. Guo, X. Xiong, W. Li, Z. Qi, and Y. Lou, "Dynamic object tracking for quadruped manipulator with spherical image-based approach," in *2023 IEEE/RSJ International Conference on Intelligent Robots and Systems (IROS)*. IEEE, 2023, pp. 727–734.

[20] O. Khatib, "A unified approach for motion and force control of robot manipulators: The operational space formulation," *IEEE Journal on Robotics and Automation*, vol. 3, no. 1, pp. 43–53, 1987.

[21] C. Ott, *Cartesian impedance control of redundant and flexible-joint robots*. Springer, 2008.

[22] J. Di Carlo, P. M. Wensing, B. Katz, G. Bledt, and S. Kim, "Dynamic locomotion in the mit cheetah 3 through convex model-predictive control," in *2018 IEEE/RSJ international conference on intelligent robots and systems (IROS)*. IEEE, 2018, pp. 1–9.

[23] X. Xiong, R. Kikuuwe, S. Kamal, and S. Jin, "Implicit-euler implementation of super-twisting observer and twisting controller for second-order systems," *IEEE Transactions on Circuits and Systems II: Express Briefs*, vol. 67, no. 11, pp. 2607–2611, 2019.

[24] C. D. Bellicoso, C. Gehring, J. Hwangbo, P. Fankhauser, and M. Hutter, "Perception-less terrain adaptation through whole body control and hierarchical optimization," in *2016 IEEE-RAS 16th International Conference on Humanoid Robots (Humanoids)*. IEEE, 2016, pp. 558–564.

[25] J.-P. Sleiman, F. Farshidian, M. V. Minniti, and M. Hutter, "A unified mpc framework for whole-body dynamic locomotion and manipulation," *IEEE Robotics and Automation Letters*, vol. 6, no. 3, pp. 4688–4695, 2021.

[26] X. Wang, "Unitree robotics," *URL https://www. unitree. com*, 2020.

[27] A. Campeau-Lecours, H. Lamontagne, S. Latour, P. Fauteux, V. Maheu, F. Boucher, C. Deguire, and L.-J. C. L'Ecuyer, "Kinova modular robot arms for service robotics applications," in *Rapid Automation: Concepts, Methodologies, Tools, and Applications*. IGI global, 2019, pp. 693–719.

[28] Y. Huang, "Srisensor," *URL https://www.srisensor.com/*, 2020.

[29] N. Koenig and A. Howard, "Design and use paradigms for gazebo, an open-source multi-robot simulator," in *2004 IEEE/RSJ international conference on intelligent robots and systems (IROS)(IEEE Cat. No. 04CH37566)*, vol. 3. IEEE, 2004, pp. 2149–2154.

[30] H. J. Ferreau, C. Kirches, A. Potschka, H. G. Bock, and M. Diehl, "qpoases: A parametric active-set algorithm for quadratic programming," *Mathematical Programming Computation*, vol. 6, pp. 327–363, 2014.

[31] M. Bloesch, M. Hutter, M. A. Hoepflinger, S. Leutenegger, C. Gehring, C. D. Remy, and R. Siegwart, "State estimation for legged robots-consistent fusion of leg kinematics and imu," *Robotics*, vol. 17, pp. 17–24, 2013.

[32] J. Carpentier, F. Valenza, N. Mansard *et al.*, "Pinocchio: fast forward and inverse dynamics for poly-articulated systems," https://stack-of-tasks.github.io/pinocchio, 2015–2021.